ELSEVIER

Bone Vol. 18, No. 2
February 1996:197–206

Dynamic Relationships of Trabecular Bone Density, Architecture, and Strength in a Computational Model of Osteopenia

R. S. SIFFERT,[1] G. M. LUO,[1] S. C. COWIN,[2] and J. J. KAUFMAN[1]

[1] *Department of Orthopaedics, Mount Sinai Medical Center, New York, NY, USA*
[2] *Department of Mechanical Engineering, The City College of the CUNY, New York, NY, USA*

A computational model was developed to study the effects of short-and long-term periods of disuse osteopenia and repair to elucidate the interrelationships between bone mass, architecture, and strength. The model is one in which the sequence of structural change events is followed in time. This temporal feature contrasts with studies of real trabecular tissue which are necessarily cross-sectional in nature and do not lend themselves to insights into the dynamic nature of the structural changes with time. In the model it was assumed that the stimulus for bone adaptation to mechanical load is the local mechanical strain rate, according to which the trabecular surfaces are differentially formed and resorbed. The effects of mechanical loading and unloading (disuse) on the cancellous bone properties were studied. The bone mass, architecture, and elastic stiffness were shown to be strongly dependent upon the period of the unloading phase, as well as the period of the reloading phase. Mechanical stiffness is demonstrated computationally to be a multivalued function of bone mass, if architecture is not accounted for. The model shows how the same value of trabecular bone mass can be associated with two or more distinct values of biomechanical stiffness. This result is the first explicit demonstration of how bone mass, architecture, and strength are related under dynamical load-bearing conditions. The results explain the empirical observation that bone mass can account for about 65% of the observed variation in bone strength, but that by incorporating measures of bony architecture into the analysis, the predictability is increased to 94%. The computational model may be used to explore the effects of different loading regimes on mass, architecture, and strength, and potentially for assistance in designing both animal and clinical bone loss studies. (*Bone 18:197–206; 1996*)

Key Words: Osteopenia; Trabecular bone density; Trabecular bone architecture; Bone strength; Bone adaptation; Mean intercept length; Boundary element method.

Introduction

Bone, as a living tissue, maintains its strength by a combination of its mass and its architectural structure.[10,25] Both mass and architecture are influenced by closely related metabolic and biomechanical factors. Techniques to accurately assess bone mineral mass in bone in vivo are well established.[18] Current clinical prediction of fracture risk is therefore based primarily on bone mass alone.[21] Nevertheless, a clearer understanding of the role played by trabecular architecture *in conjunction* with bone mass is important for ultimately dealing, as effectively as possible, with bone loss disorders, particularly osteoporosis.[17]

Trabecular bone is a highly complex material, whose apparent elastic modulus is a function of its density.[3,20] The actual modulus of a trabeculum, the tissue level modulus, has been estimated over the last century to be between 1 and 20 GPa. It has only recently been determined to be in the range of 5–8 GPa, we use 7 GPa in this study.[10] The variation in the apparent elastic modulus is dependent upon many factors, including anatomic site, species, age, loading direction, and disease state.[10] Bone mass is the primary factor contributing to bone strength. In vitro studies demonstrate a quantitative relationship between bone mass and biomechanical stiffness and strength.[3,20] Other factors besides bone mass are also important with respect to the biomechanical properties of bone. For example, the apparent density of trabecular bone accounts for only about 65% of the observed variation in overall strength.[20] This can be increased up to 94% by including in the model a measure of bone architecture known as fabric, a quantification of the relative degree of structural anisotropy.[5,26,27] Parfitt[19] has shown that changes in trabecular bone microstructure are related to increased incidence of osteoporotic fractures. It has been shown that the number and thickness of trabeculae decrease with decreasing density (i.e., with increasing age), and that the intertrabecular spaces increase.[2] Mosekilde and coworkers[15] showed that the modulus of human trabecular bone in the load-bearing direction decreased significantly with age, at the rate of about 17% per decade. In addition, they have reported that the strength anisotropy that exists for vertebral trabecular bone increases with aging.[16]

Architectural in vivo assessment techniques are significantly less developed, although recent studies have demonstrated the relative importance of architecture and mass as determinants of bone strength.[25] Several attempts at developing in vivo techniques for assessing bone architecture have also been reported. Changes in radiographic trabecular patterns of the human os calcis under biomechanical disuse were detected using various textural features.[7] These studies were extended to computed tomography scans of human vertebral bodies in an attempt to more accurately predict strength, compared with using bone mass alone.[8,9]

The dynamic relationships existing between bone mass, ar-

Address for correspondence and reprints: Dr. Robert S. Siffert, Department of Orthopaedics, MS 1188, The Mount Sinai School of Medicine, One Gustave L. Levy Place, New York, NY 10029.

8756-3282/96/$15.00
SSDI 8756-3282(95)00446-7

Bone Vol. 18, No. 2
February 1996:197–206

chitecture, and biomechanical properties has received considerably less attention. Part of the reason for this arises out of the complexity and cost of carrying out long-term animal or clinical studies. Another reason is the difficulty in assessing biomechanical and architectural features in vivo. Several studies have described changes that occur over time under various conditions. Animal experiments involving disuse and recovery have been reported since the 1970s; these studies very strongly influenced the computational adaptation reported here. Using rats, Lindgren and Mattsson[12] concluded that bone mass could not be recovered after long-term disuse. Using young adult and old beagle dogs, Jaworski and Uhthoff[6] showed that full recovery of bone mass was possible if remobilization occurred early enough, and, more recently, Schaffler and Pan,[24] using adult female beagles, have shown that there is a point of no return between 12 and 20 weeks of disuse where continued disuse causes loss of trabecular elements and the bone mass cannot be recovered. They noted that bony architecture associated with disuse-induced bone loss is different at different time points in the immobilization history. For up to 12 weeks of disuse, loss of trabecular bone mass occurs by resorption on all bone surfaces, resulting in an overall thinning of trabeculae. After 12 weeks of disuse, osteoclastic activity has been shown to lead to perforation and removal of trabeculae.[24] These results are consistent with the observations of Mosekilde et al. [15] and they represent the type of results that are modeled here. The strain values used in the bone adaptation models employed here come from Lanyon[11] and Rubin and Lanyon,[22,33] who measured the values of axial strain in structural long bones of many species and found that net bone resorption will occur when compressive strains are less than 0.001, and that net deposition will occur when compressive strains are greater than 0.003.

This report describes a tissue level, as opposed to a continuum level, computational model which can simulate physical changes that occur during alternate periods of bone disuse and subsequent reloading. An objective is to identify the relative roles played by mass and architecture as reflected in bone stiffness and strength. An overall objective is to better understand the dynamic, i.e., time-dependent, relationships between trabecular architecture, mass, and strength, and to also provide a means for exploring in further detail these complex relationships. Another long-term objective is to develop a tool in association with experimental and clinical observations to predict the effects of particular mechanical loading regimes, and of exogenous therapeutic agents on the biomechanical properties of cancellous bone structures.

Methods

In this section we describe the tissue level computational model which we use to compute the evolution of trabecular bone mass, architecture, and biomechanical properties under specific loading regimes. We will also describe the methods used to assess the properties of the trabecular bone structure.

The model is based on the principle that bone turnover process is a surface phenomenon in which osteoclastic thinning of existing trabeculae during catabolic periods and then osteoblastic thickening of remaining trabeculae during the repair stage occur. Recognizing the many metabolic, nutritional, environmental, and genetic factors that are involved as well, the model permits an evaluation of the stiffness of bone as a whole under controlled conditions of simulated osteopenia and repair, as well as the relative role played by mineral mass and trabecular architecture.

The computational model involves several components, the boundary element method, the local adaptation criterion, the initial trabecular structure used, and the applied loading regime. The boundary element method is used to computationally evaluate the local stresses and strains at each point near the trabecular surface undergoing strain adaptation for a specific load, under assumptions that the trabecular bone material is linearly elastic and isotropic. The boundary element method is implemented according to the description found in Banarjee and Butterfield.[1]

The strain rate stimulus values at each point near a potential strain adaptation surface is used to determine whether or not strain adaptation occurs at that surface. In this approach, the thickness of a trabeculum increases, decreases, or remains the same, according to the value of the local strain rate stimulus S. The implementation and justification for strain rate as an adaptation stimulus has been presented by Luo et al. [13] In expressing this criterion, U is used to denote the velocity of the bone surface (U 0 is deposition and $U < 0$ is resorption), and S_0 is used to denote an adaptation equilibrium value of the stimulus, S thus:

$$U = \begin{cases} K_1(S - S_{0-}), \text{ if } S < S_{0-} \\ 0, \text{ if } S_{0-} < S < S_{0+} \\ K_2(S - S_{0+}), \text{ if } S_{0+} < S \end{cases}.$$

If S is within the range S_{0-} to S_{0+} there is no adaptation. This equation may be considered as an additional constitutive equation that specifies the velocity of movement of the exterior bone surfaces. A plot of the adaptation surface velocity against the stimulus is shown in **Figure 1.** In this characterization, S_{0+} is the value of the strain rate stimulus above which deposition occurs, and S_{0-} is the value of the stimulus below which resorption occurs. The strain rate stimulus domain, $S_{0-} = 0.00044 < S < S_{0+} = 0.00132$, is the adaptation equilibrium domain, in which no net deposition or resorption occurs. In this analysis the adaptation rate constants $K_1 = K_2 = K$, are set equal to 1 mm per unit of time where the unit of time is unspecified. In the calculations presented, the number of steps in the calculation is more significant that the time unit, and the results are valid for all selections of the time unit. For example, letting the time unit equal 1 day so that $K = 1$ mm/day and assuming the strain rate, S, is 50% greater than S_{0+}, then the adaptation velocity is about 0.7 μm/day. This is of the same order as reported by Chow et al.[4]

Once the entire trabecular surface is adapted according to the velocity U during a brief time interval for each point on the adapting surface, the process of calculating the strain rate stimu-

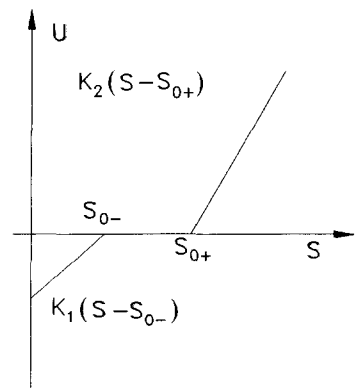

Figure 1. The surface bone adaptation velocity U as a function of the surface bone adaptation stimulus S. In this description, S_{0+} is the value of the strain rate stimulus above which deposition occurs, and S_{0-} is the value of the stimulus below which resorption occurs. The strain rate stimulus domain, $S_{0-} = 0.00044 < S < S_{0+} = 0.00132$, is the adaptation equilibrium domain, in which no net deposition or resorption occurs.

lus and surface velocity function is repeated. The values associated with bone mass, architecture, and mechanical properties at each time point of the adaptation process are evaluated according to the methods discussed in the following paragraphs.

The idealized trabecular bone model used in this study is shown in **Figure 2.** Due to the periodicity and the symmetry of the model only one unit shown in Figure 2 is computationally simulated. The results obtained on this one unit are then directly extended to the overall structure. The elastic constants for solid bone (i.e., the trabecular bone material) are the Young's modulus, E_s, assumed to be 7 GPa and the Poisson's ratio, ν_s, assumed to be 0.28. Because linear elasticity was employed in this study, the ratio of Young's modulus and external load is important, not their values. If we increase or decrease the values of Young's modulus and external load proportionally, identical strain adaptation processes will occur. The load, P_y, is externally applied on the structural unit in the vertical direction, while the load, P_x, on the structural unit in the horizontal direction is created by the Poisson effect.

The loading history of the bone tissue is assumed to be that characteristic of normal walking. Thus, a periodic load with a period of 0.5–1 sec (1–2 Hz) is assumed to be applied to the trabecular structure. The surface bone adaptation strain rate stimulus is given by twice the maximum amplitude of the periodic strain signal.[13]

To initialize the computational process, maximum loads P_y = 1.9 N (equivalent to an average stress of 3.8 MPa) and P_x = 0.5 P_y (equivalent to an average stress of 0.95 MPa) are applied to the idealized trabecular structure. Through use of the boundary element procedures, together with the constitutive relationship of Equation (1), the structural unit is computationally adapted until adaptation equilibrium, referred to as adaptation equilibrium state (a), is reached. This equilibrium structure serves as the initial condition for all of the following computer simulations.

Two different loading regimes are used to simulate disuse osteopenia. In the first, the external load is set to zero for a relatively short period of time before restoring the load to its original value. In the second, a significantly longer period of disuse is simulated before restoring the original external load. In both disuse processes, the model was initialized using the adaptation equilibrium state (a) as described in the preceding paragraph. The two processes are summarized in what follows.

Short-Term Disuse Process

Step 1. Simulate disuse by removing all loads, i.e., setting P_x = P_y = 0, and let bone resorb, stopping the process before any horizontal trabeculae have resorbed.

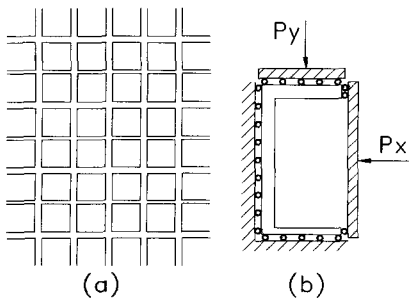

Figure 2. The idealized trabecular bone model employed in this study; (a) the complete structure and (b) the unit cell employed in the computational algorithm.

Step 2. Simulate the recovery process by reapplying the load P_y = 1.9 N and P_x = 0.5 P_y until a new adaptation equilibrium, referred to as adaptation equilibrium state (b), is reached.

Long-Term Disuse Process

Step 1. Simulate disuse by removing all loads, i.e., setting P_x = P_y = 0, and let bone resorb until some horizontal trabeculae have resorbed.

Step 2. Simulate the recovery process by reapplying the load P_y = 1.9 N and P_x = 0.5 P_y until a new adaptation equilibrium, referred to as adaptation equilibrium state (c), is reached.

Bone strain adaptation alters bone structure, thereby causing changes in its strength. Measurement of the biomechanical strength changes in the trabecular structure were made for the three strain adaptation equilibrium states, namely, the initial state and the adaptation equilibria states following the short- and long-term disuse processes, respectively. The strength of the trabecular structures was characterized by the maximum principal strain in the sample. For each adapted equilibrium structure, we report the maximum principle strain as a function of applied loading angle **(Figure 3),** relative to the maximum principal strain value obtained for O° loading in the initial structural equilibrium state. For a sample of trabecular bone with homogeneous and orthotropic material properties i.e., Young's moduli E_x, E_y, Poisson's ratios ν_{xy}, ν_{yx}, and shear modulus G, the maximum principal strain for the three adapted equilibrium structures can be computationally determined as a function of load amplitude and loading angle, θ. In this calculation, Poisson's ratio ν_{yx} is assumed to be 0.2.

Before presenting the results of this study, we explain some terms that are used. The *volume ratio* is defined as the volume of the space occupied by solid bone per unit volume. *Mean Intercept Length* (MIL) is defined as the inverse of the number of intersections per unit length of a test line with the bone-void boundary.[27] **Figure 4** demonstrates how the MIL is measured in a typical cancellous bone specimen. MIL is a function of angular orientation, i.e., the angle at which the mean intercept lengths are measured. Thus bone oriented primarily in the vertical direction will have a MIL value distinct from that for the horizontal direction. The MIL function is a measure of the structural anisotropy associated with a sample of trabecular bone. In this study, we characterize the architecture of trabecular bone by the ratio of the MIL in the vertical direction to the MIL value in the hori-

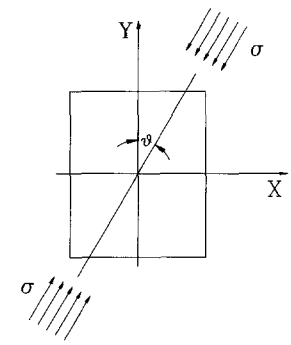

Figure 3. The strength test model. The strength of a trabecular structure is characterized by its maximum principal strain, i.e., for a given bone sample when the maximum principal strain is higher than a prespecified value, we assume that the sample will fail. For each adaptation equilibrium, we report the maximum principal strain, as a function of applied loading angle.

Bone Vol. 18, No. 2
February 1996:197–206

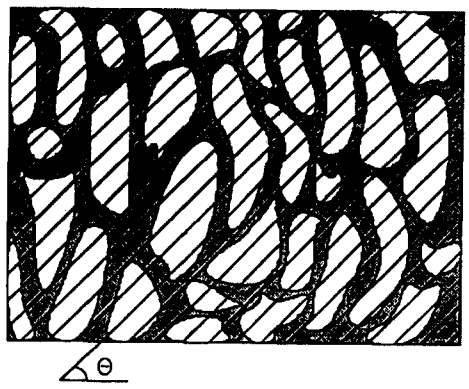

Figure 4. Test lines superimposed on a cancellous bone specimen. The test lines are oriented at the angle, υ. The mean intercept length measured at this angle is denoted by MIL(υ).

zontal direction, which is termed the *mean intercept length ratio* (MILR). *Stiffness* is directly proportional to Young's modulus for a solid bar, while Young's modulus is measured in the following way: If a bar with uniform cross-section shape and area A is uniaxially loaded longitudinally by a force P, the Young's modulus is defined as $P/(Ad)$, where d, assumed to be small, is the elongation of the bar per until length. *Strength* is defined as P_{max}/A, where P_{max} is the maximum force that the bar can sustain. The important point to remember is that stiffness is a measurement of structural elasticity while strength is the stress at which the material breaks or yields.

Results

The response of the same initial trabecular equilibrium structure to both a short-term and a long-term disuse process was computationally determined. **Figure 5** shows pictorially the changes induced by short-term disuse. The initial bone is the sum of the shaded and unshaded areas, the removed bone is shaded, and the remaining bone is unshaded. As may be seen, all trabecular surfaces are thinned, since the local strain rate is below the value for which bone begins to resorb and the disuse process has been stopped prior to any of the trabeculae being completely resorbed. Once the external load is reapplied, the structure remodels to a new equilibrium state as shown in **Figure 6.** As may be seen, a thickening of trabeculae is observed to occur only on the longitudinal (vertical) trabeculae. This is due to the nonuniform distribution of induced strain rate on the trabecular surfaces, and the fact that the strain rate on the transverse trabeculae falls in the inactive region of the strain rate adaptation function (Figure 1). Thus, the strain rates induced on the transverse or crossbracing trabeculae are such that little adaptation occurs at these sites.

The long-term disuse process is shown in **Figure 7** and **Figure 8.** As may be seen, the longer period of mechanical disuse leads to some of the transverse trabeculae becoming completely resorbed (Figure 7). During repair, i.e., reloading, significant thickening occurs only on the vertical or main load-bearing trabeculae. Note that bone growth is observed to occur only on pre-existing trabeculae. Note also that the amount of thickening of the longitudinal trabeculae is greater in the long-term model (Figure 8), compared with that which occurs for the short-term disuse model (Figure 8). Again, this is due to the specific amount of induced strain rate for a given external load over the specified time interval.

The qualitative and graphical changes in the trabecular structures observed for the long-and short-term disuse processes can be quantified using the mass, architectural, and biomechanical features as described earlier. **Figure 9** displays the time evolution of bone mass for the long-and short-term disuse processes. As may be seen, there is a uniform decrease in bone mass during disuse, with a significant increase following the reapplying of the external load. In both cases, the final equilibrium mass values do not return to their original value, and the long-term disuse produces a greater overall bone loss. This finding is consistent with both experimental and clinical radiologic observations during periods of disuse and repair.[7]

The mean intercept length ratio (MILR) is shown in **Figure**

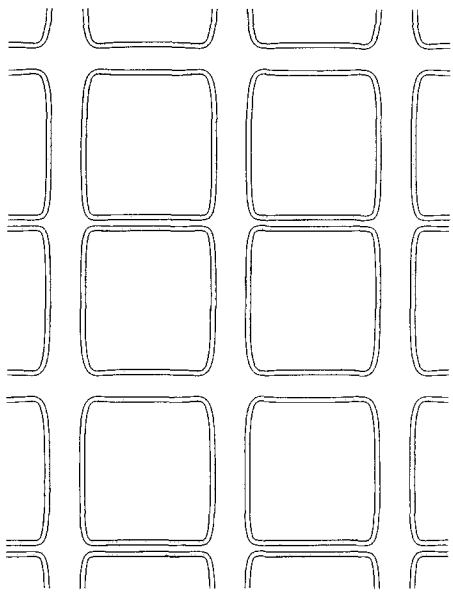

Figure 5. Overall model before surface resorption of trabeculae and remaining trabeculae (unshaded) after bone removal (shaded).

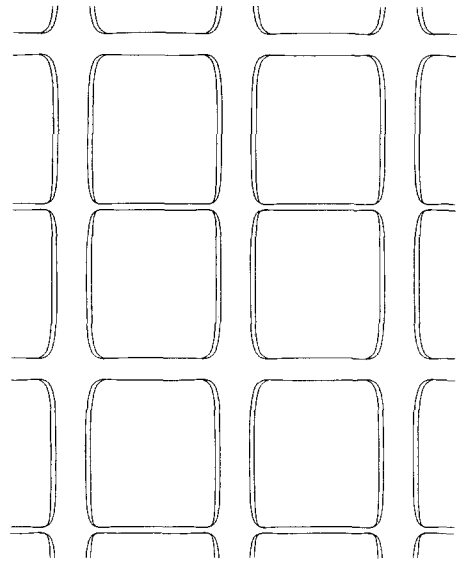

Figure 6. Model after short-term absorption and repair by trabecular thickening (shaded). The longitudinal trabeculae, receiving major weight-bearing stresses, have thickened more than the less stressed horizontal trabeculae.

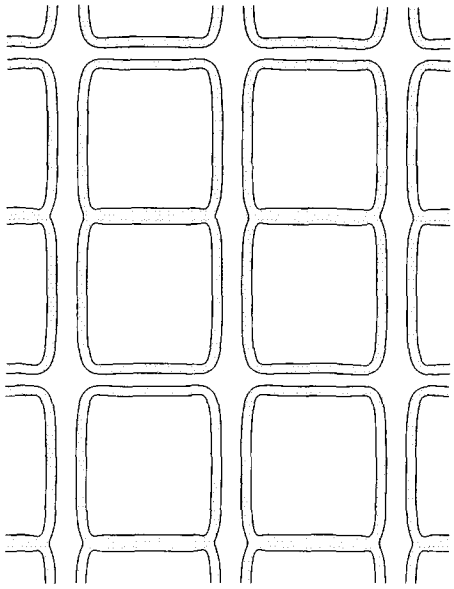

Figure 7. Model indicating greater amount of absorption of trabecular surface (gray) after long-term relief of longitudinal load to the point that some cross-bracing trabeculae have disappeared.

10 as a function of time. In this quantitative representation of trabecular structure, the short-term disuse model does not produce a significant degree of change during the entire time course. On the other hand, the long-term disuse produces about a 90% increase in the MILR, indicating significant architectural changes in the trabecular structure.

Figures 11 and 12 display the time dependent changes in vertical (E_y) and horizontal (E_x) stiffnesses of the trabecular structures, respectively, for the long-and short-term disuse processes. Figure 11 shows that the vertical stiffness decreases more for the long-term compared with the short-term disuse process, but that the vertical stiffness returns to nearly its initial value, for both the long and short disuse periods. In contrast, Figure 12 demonstrates that the horizontal stiffness is significantly reduced in both the long-term and short-term disuse processes, compared with the initial horizontal stiffness value. However, the long-term disuse produces a significantly greater decrease in E_x than does the short-term disuse process, due to loss of horizontal trabeculae.

Figure 13 displays the vertical stiffness, E_y, versus bone mass for the two disuse processes. In this depiction, time is implicit and increases monotonically along the stiffness-mass trajectory from the initial to the final point. It is of a particular interest to note that the relationship between bone mass and vertical stiffness in this computational model is multivalued. That is, for a specific value of bone mass, more than one value of vertical stiffness may be found. Likewise, for a specific value of vertical stiffness, more than one value of bone mass may be found. This multivalued nature is more predominant in the long-term disuse process. **Figure 14** shows horizontal stiffness, E_x, versus bone mass, and a similar multivalued relationship is observed here as well.

Table 1 summarizes the discussed changes quantitatively for bone mass, MILR, E_x, and E_y, and also for the shear modulus, G, for the three equilibrium states of the trabecular structure. The three adaptation equilibrium states are denoted by (a), (b), and (c), respectively, where (a) indicates the initial adaptation equilibrium, (b) the adaptation equilibrium for a short-term disuse process, and (c) the adaptation equilibrium for a long-term disuse process. The percent change of the trabecular features for adaptation equilibria (b) and (c) are also displayed in Table 1 by using the values of the respective parameters in the adaptation equilibrium state (a) as reference values. For example, the MILR is 1.16 for equilibrium state (a), while it is 1.23 and 2.18 for equilibrium states (b) and (c), respectively. Thus, there is a significant increase in the structural anisotropy as measured by MILR associated with the long-term disuse process.

In **Table 2,** the variations of the maximum principal strain are listed for the three adaptation equilibrium states and for five different loading angles. In the calculation of these principal strain values, the adaptation equilibrium state (a) at O° is used as a reference. As Table 2 shows, there is a dramatic increase in the maximum principal strain as the angle of loading increases from O°, for both the short-term and long-term disuse processes. However, the increase is highest for the long-term disuse process. The data in Table 2 indicate that the strength of the structure is severely compromised in both loading regimes to off-vertical loads, and that the greatest compromise occurs for the long-term disuse process. For example, at a loading direction of 2°, the relative increase in the maximum principal strains are 9.1%, 41.7%, and 184.3% for equilibrium states (a), (b), and (c), respectively. This means that at an off-axis loading of only 2°, the long-term disuse state (c) has about twice the strain induced as compared with the short-term disuse state (b). Thus, the combination of mass and architectural changes induced by the long-term disuse process lead to a more marked decrease in its associated biomechanical strength, compared with those induced by the short-term disuse process.

Discussion

The numerical simulations, as in Table 1 show that the disuse processes can significantly change the volume ratio, −12% for short-term disuse (b) and −20% for long-term disuse (c), respectively; Young's modulus in the horizontal direction, −36% for

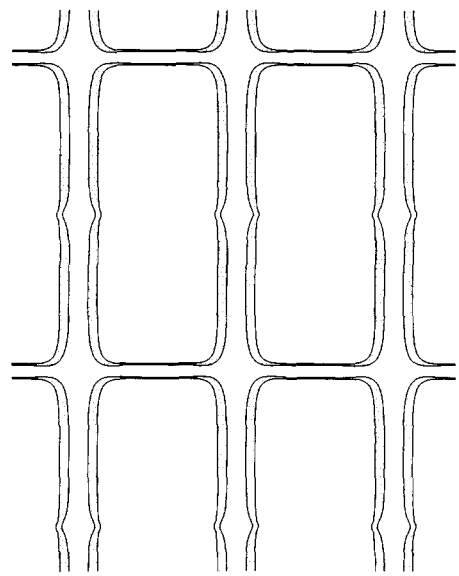

Figure 8. Repair of the long-term disuse model after complete resorption of some cross-bracing trabeculae, which do not reappear because remaining trabeculae serve as templates on which new bone will form (gray).

Bone Vol. 18, No. 2
February 1996:197–206

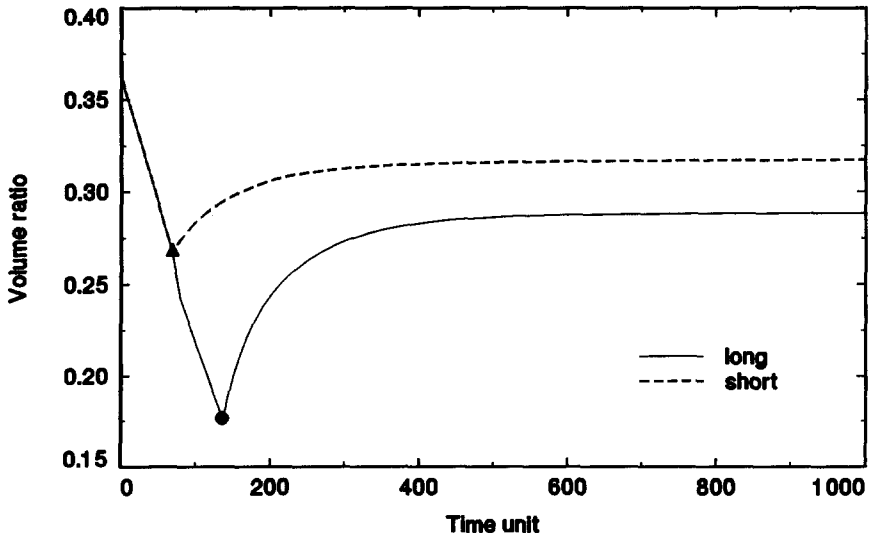

Figure 9. Bone mass as a function of time for the adaptation model with a long-term (solid line) and short-term (dashed line) disuse. The solid triangle indicates when the short-term disuse ended and the solid circle indicates when the long-term disuse ended, in which both cases were followed by reloading of the structure. These symbols have the same meaning in all subsequent figures. Note that the bone mass does not return to its original value, and that the long-term disuse results in a greater reduction of bone mass.

(b) and −62% for (c) respectively; and the shear modulus, −57% for (b) and −85% for (c), respectively. However, the change in Young's modulus in the vertical direction, the main external loading direction, is negligible, −2% for (b) and −3% for (c), respectively. These results imply that trabecular bone may become much less able to withstand multidirectional loading in cases when bone mass is reduced. This loss of mechanical stability is enhanced when the bone loss leads to significant changes in the trabecular microstructure, as shown in the comparison between the short-term and long-term disuse models.

The strength analysis, as provided in Table 2, also is consistent with these statements. Table 2 shows that the trabecular bone of all three adaptation equilibrium states has almost the same maximum principal strains under vertical loading. The maximum principal strain can be used as a strength measurement, i.e., when the maximum principle strain in a trabecular structure is higher than a given value the sample will fail. The results presented in Table 2 imply that the three adaptation equilibrium states have almost the same vertical strength independent of the bone having been in a disuse process. However, if the applied load is off the vertical direction, the maximum principal strain in the structure with disuse is much higher than one without any disuse, with the same external load amplitude. This would imply that the trabecular bone structure with disuse has a much higher failure risk than one without any disuse. Moreover, the bone structure with the long-term disuse process (c) is much more sensitive to the loading orientation than the one with the short-term disuse process (b). This suggests the need for properly timed intervention in bone loss disorders, or for preventive measures to be instituted as early as possible.

Many investigations utilizing bone specimens as well as clinical studies have attempted to elucidate the interrelationships between bone mass, architecture, and strength. The cross-sectional nature of those studies does not lend itself to establishing insights into the dynamic nature of changes that occur in trabecular bone structures over time. To address this limitation, the computational approach described in this article was developed. This approach attempts to model the temporal changes that occur in a specified trabecular model structure under distinct loading conditions. The model suffers from several limitations itself. First, it is two-dimensional and therefore only partially representative of the complex three-dimensional changes that occur in trabecular

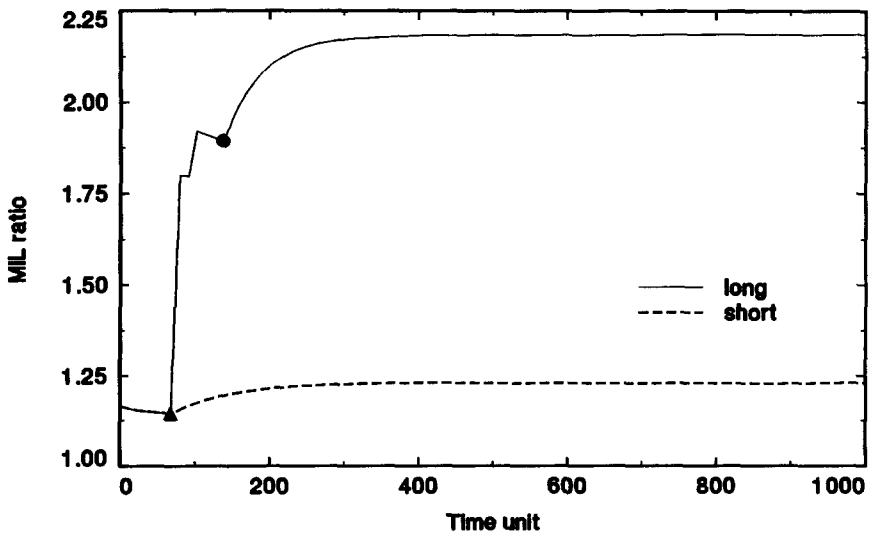

Figure 10. The MIL ratio as a function of time for the adaptation models with a long-term (solid line) and short-term (dashed line) disuse. Note the significantly greater change in architecture by the long-term disuse process.

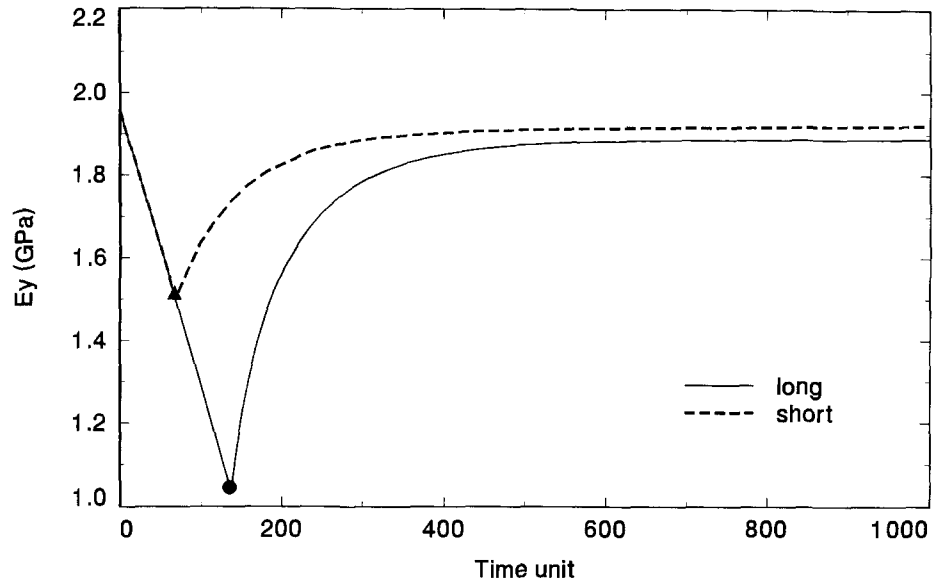

Figure 11. The Young's modulus, E_y in the vertical direction (vertical stiffness) as a function of time for the adaptation model with a long-term (solid line) and short-term (dashed line) disuse. Note that, in both cases, the moduli return almost to their initial values, after experiencing a large reduction during the disuse period.

bone. Second, the structure used in the simulations is highly simplified and not typical of the kinds of trabecular architecture actually existing. Third, the model assumes that strain rate is the determining factor in terms of bone adaptation. Although this assumption is still a point of debate, the results of this study would not be significantly affected by choice of another but similar adaptation stimulus, such as strain magnitude, for the conditions described herein. However, this model could eventually serve to test the strain rate hypothesis based on its predictions for a specific experimental set of conditions. Finally, the model as designed does not take into account the complex physiological and biological processes involved in bone adaptation. For example, the model assumes a normal state of health in which reformation of bone on existing surfaces will occur in response to mechanical forces. In fact, this assumption may need to be modified depending upon osteoblastic capability of repair in osteoporotic bone. Older individuals may have diminished osteogenic potential and fewer trabeculae to serve as a scaffold for new bone formation. Therefore, a period of life may arise when progressive osteopenia will occur independent of mechanical stimulation. None of these considerations are presently accounted for in the computational model.

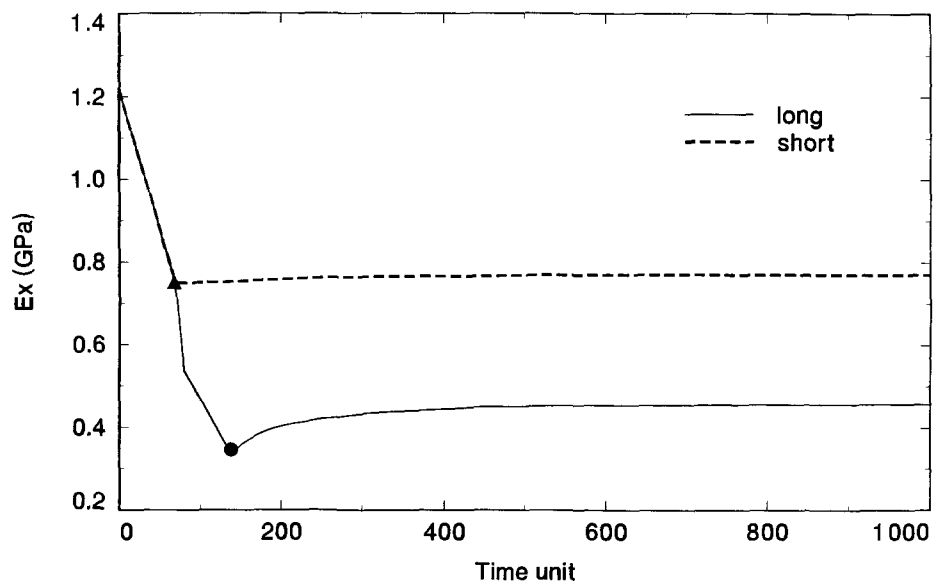

Figure 12. The Young's modulus, E_x, in the horizontal direction (horizontal stiffness), as a function of time for the adaptation model with a long-term (solid line) and short-term (dashed line) disuse. In contrast with Figure 10, the horizontal moduli do not return to their initial values upon reloading, and that the long-term disuse process results in significantly greater reduction in horizontal modulus than the short-term disuse.

Bone Vol. 18, No. 2
February 1996:197–206

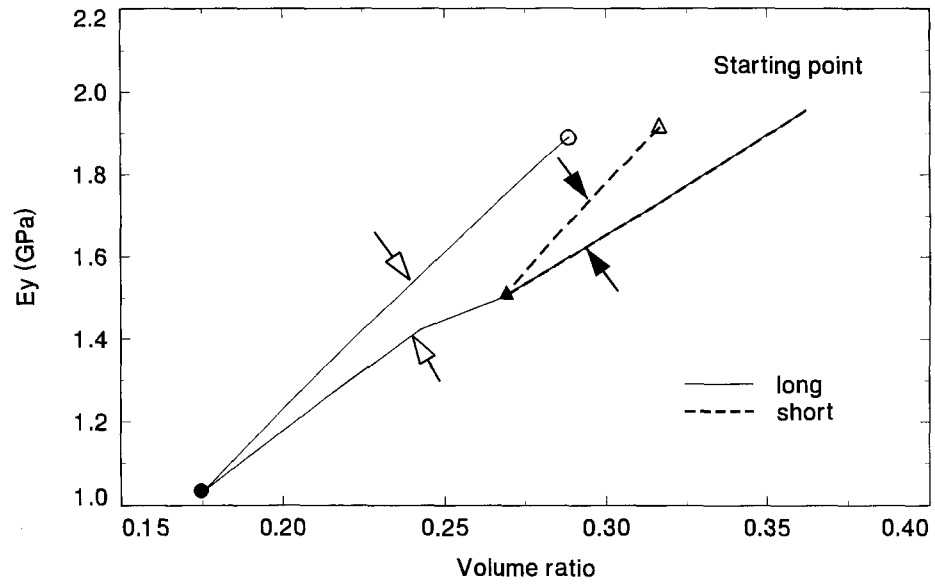

Figure 13. The Young's modulus in vertical direction (vertical stiffness) versus bone mass for the adaptation model with a long-term (solid line) and short-term (dashed line) disuse. Solid triangle mark indicates when the short-term disuse ended and solid circle mark indicates when the long-term disuse ended. Both the empty triangle and empty circle indicate final adaptation equilibrium. Note that the dashed and solid lines are coincident during the initial stages of disuse. The arrow pairs indicate points at which the structure has approximately the same mass but different stiffness values.

In spite of these limitations, the computational model and the results presented can shed some light on the bone adaptation process. Several experimentally observed phenomena do appear to be consistent with some of the results obtained here. For example, Jaworski and Uhthoff[6] observed thicker trabeculae after disuse and recovery, suggesting that trabeculae were lost during disuse and the remaining trabeculae were thickened during recovery. Consistent with the results reported here, Schaffler and Pan[24] observed that the bony architecture associated with disuse-induced bone loss is different at different time points in the immobilization history. They noted that, for up to 12 weeks of disuse, loss of trabecular bone mass occurs by resorption on all bone surfaces, resulting in an overall thinning of trabeculae. After 12 weeks of disuse, osteoclastic activity perforates and removes trabeculae.[24] Another important observation is that the computational model demonstrates why bone mass often does not serve to estimate accurately bone stiffness and strength. In this regard, the model is also consistent with the experimental

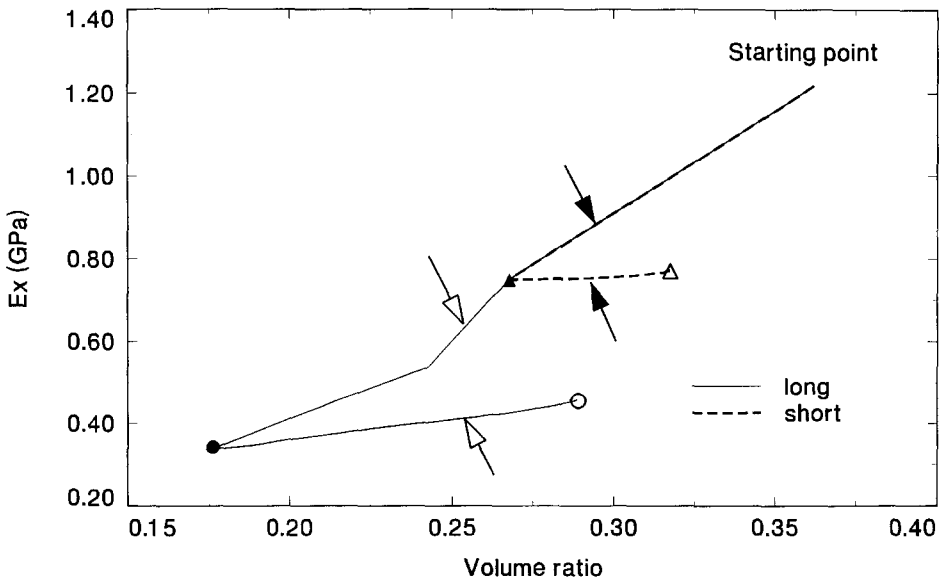

Figure 14. The Young's modulus in the horizontal direction (horizontal stiffness) versus bone mass for the adaptation model with long-term (solid line) and short-term (dashed line) disuse processes. Solid triangle mark indicates when the short-term disuse ended and solid circle mark indicates when the long-term disuse ended. Both empty triangle and empty circle marks indicate final adaptation equilibrium. Note that the dashed and solid lines are coincident during the initial stages of disuse. The arrow pairs indicate points at which the structure has approximately the same mass but different stiffness values.

Table 1. The values of five measures of the mechanical structure of trabecular bone for three different adaptation equilibrium states: (a) initial adaptation equilibrium; (b) adaptation equilibrium after short-term disuse; and (c) adaptation equilibrium after long-term disuse[a]

	Volume ratio	MIL ratio	E_x (GPa)	E_y (GPa)	G (GPa)
(a)	0.362	1.16	1.22	1.96	0.100
(b)	0.317 (−12%)	1.23 (+6%)	0.770 (−36%)	1.92 (−2%)	0.0431 (−57%)
(c)	0.289 (−20%)	2.18 (+88%)	0.459 (−62%)	1.89 (−3%)	0.0147 (−85%)

[a] The relative percent changes of the measures are calculated by taking the values for adaptation equilibrium state (a) as reference.

results of Mosekilde and Viidik[16] who showed that the anisotropy of vertebral trabecular bone increases with age.

Although it has been previously suggested[14,19] that architecture plays a role in the biomechanics of clinical bone loss, this is the first attempt which provides an explicit and quantitative characterization of the temporal processes involved in bone adaptation. The results portray, for example, how clinical bone integrity, i.e., strength and stiffness, may be largely maintained in spite of significant reductions in bone mass. Conversely, the results indicate how architectural changes in osteopenic trabecular bone can lead to profound reductions in bone strength compared with trabecular bone of similar bone density. Since the normal process of bone turnover consists of both absorption and formation, measurement of bone mass alone may coincide with different trabecular patterns and stiffness depending upon the biodynamics that exist at the time. Accordingly, clinical bone densitometry measurements may not provide accurate characterizations of bone strength.

Summary

This study has described the implementation of a simplified computational model of trabecular bone adaptation response to load regimes corresponding to short and long-term stages of disuse osteopenia and repair. The model elucidates selected aspects of trabecular bone adaptation and the interrelationships of bone mass, architecture, biomechanical stiffness, and strength. Under controlled situations, the model trabecular structure responds predictably in tracing changes during the development of osteopenia and during attempts at repair. A model simulating osteopenia of disuse will repair to a trabecular architecture different from the original trabecular architecture. The duration of the osteopenic stage is the main determinant of the final architectural changes, indicating the need for properly timed preventive measures. The model also demonstrates quantitatively that stiffness of trabecular bone is a function of both mass and architectural structure. This ambiguity or multivalued nature may be able to be reduced by specifying the architectural state of trabecular bone at a particular point in time. Finally, the computational paradigms developed in this article may serve as guides in identifying pertinent animal experiments and developing timely clinical preventive and therapeutic programs.

Table 2. Maximum principal strain increases when either the loading angle, θ, changes from 0° to 10° or the adaptation equilibrium state changes from (a) to (c)[a]

		Loading angle, θ				
		0°	1°	2°	5°	10°
(a)	Maximum strain	0.0%	2.5%	9.1%	44.4%	118.4%
(b)	Maximum strain	1.8%	13.9%	41.7%	149.0%	337.3%
(c)	Maximum strain	3.5%	74.7%	184.3%	527.3%	1090.8%

[a] The numbers show the relative increases of the maximum principal strain by taking the maximum principle strain of adaptation equilibrium state (a) at zero loading angle as reference.

References

1. Banerjee, P. K. and Butterfield, R. Boundary element methods in engineering science. New York: McGraw-Hill; 1981.
2. Bergot, C., Laval-Jeantet, A. M., Preteux, F., and Meunier, A. Measurement of anisotropic vertebral trabecular bone loss during aging by quantitative image analysis. Calcif Tissue Int 43:142–149; 1988.
3. Carter, D. R. and Hayes, W. C. The compressive behavior of bone as a two phase porous structure. J Bone Jt Surg 59:954–962; 1977.
4. Chow, J. W. M., Jagger, C. J., and Chambers, T. J. Characterization of osteogenic response to mechanical stimulation in cancellous bone of rat caudal vertebrae. Am J Physiol 265:E340–E347; 1993.
5. Harrigan, T. P. and Mann, R. W. Characterization of microstructural anisotropy in orthopaedic materials using a second rank tensor. J Mat Science 19:761–766; 1984.
6. Jaworski, Z. F. G. and Uhthoff, H. K. Reversibility of nontraumatic disuse osteoporosis during its active phase. Bone 7:431–439; 1986.
7. Kaufman, J. J., Mont, M. A., Hakim, N., Ohley, W., Lundahl, T., Soifer, T., and Siffert, R. S. Texture analysis of radiographic trabecular patterns in disuse osteopenia. Trans Orthopaedic Res Soc 12:265; 1987.
8. Kaufman, J. J., Hakim, N., Nasser, P., Mont, M., Klion, M., Hermann, G., Pilla, A. A., and Siffert, R. S. Digital image processing of vertebral computed tomography scans for mechanical strength estimation. Trans Orthopaed Res Soc 13:230; 1988.
9. Kaufman, J. J., Nasser, P., Mont, M., Hakim, N., Pilla, A. A., and Siffert, R. S. Texture analysis of vertebral computed tomography scans improve trabecular strength estimation. Trans Orthopaed Res Soc 14:264; 1989.
10. Keaveny, T. M. and Hayes, W. C. A 20-year perspective on the mechanical properties of trabecular bone. Trans ASME 115:534–542; 1993.
11. Lanyon, L. E. Functional strain as a determinant for bone remodeling. Calcif Tissue Int 36:S56–S61; 1984.
12. Lindgren, U. and Mattsson, S. The reversibility of disuse osteoporosis. Calcif Tissue Res 23:179–184; 1977.
13. Luo, G. M., Cowin, S. C., Sadegh, A. M., and Arramon, Y. P. Implementation of strain rate as a bone remodeling stimulus. J Biomech Eng 117:329–338; 1995.
14. Martin, R. B. Porosity and specific surface of bone. CRC Crit Rev Biomed Eng 10:179–222; 1984.
15. Mosekilde, L., Mosekilde, L., and Danielsen, C. C. Biomechanical competence of vertebral trabecular bone in relation to ash density and age in normal individuals. Bone 8:79–85; 1987.
16. Mosekilde, L. and Viidik, A. Correlations between the compressive strength of iliac and vertebral bone in normal individuals. Bone 6:291–295; 1985.
17. NIH Consensus Development Panel Consensus Conference Osteoporosis. JAMA 252:799–802; 1984.
18. Ott, S. M., Kilcoyne, R. F., and Chestnut, C., III. Ability of four different techniques of measuring bone mass to diagnose vertebral fractures in postmenopausal women. J Bone Miner Res 2:201–210; 1987.

Bone Vol. 18, No. 2
February 1996:197–206

19. Parfitt, A. M. Trabecular bone architecture in the pathogeneses and prevention of fracture. Am J Med 82:68–72; 1987.
20. Rice, J. C., Cowin, S. C., and Bowman, J. A. On the dependence of the elasticity and the strength of cancellous bone on apparent density. J Biomech 22:155–168; 1988.
21. Riggs, B. L. and Melton, L. J. Involutional osteoporosis. N Engl J Med 314:1676–1686; 1986.
22. Rubin, C. T. and Lanyon, L. E. Regulation of bone formation by applied dynamic loads. J Bone Jt Surg 66A:397–410; 1984.
23. Rubin, C. T. and Lanyon, L. E. Osteoregulatory nature of mechanical stimuli: function as a determinant for adaptive bone remodeling. J Orthoped Res 5:300–307; 1987.
24. Schaffler, M. B. and Pan, H. Q. Alterations of trabecular microarchitecture during immobilization-induced bone loss. Trans Orthopaed Res Soc 17:239; 1992.
25. Turner, C. H. and Cowin, S. C. Dependence of elastic constants of an anisotropic porous material upon porosity and fabric. J Mat Sci 22:3178–3184; 1987.
26. Turner, C. H., Rho, J. Y., Ashman, R. B., and Cowin, S. C. The dependence of elastic constants of cancellous bone upon structural density and fabric. Trans Orthopaed Res Soc 13:74; 1988.
27. Whitehouse, W. J. The quantitative morphology of anisotropic trabecular bone. J Micros 101:153–168; 1974.

Date Received: February 27, 1995
Date Revised: October 20, 1995
Date Accepted: October 20, 1995